ARL-TR-8163 ● SEP 2017

US Army Research Laboratory

Development of Cranial Bone Surrogate Structures Using Stereolithographic Additive Manufacturing

by Jared M Gardner and Thomas A Plaisted

NOTICES

Disclaimers

The findings in this report are not to be construed as an official Department of the Army position unless so designated by other authorized documents.

Citation of manufacturer's or trade names does not constitute an official endorsement or approval of the use thereof.

Destroy this report when it is no longer needed. Do not return it to the originator.

ARL-TR-8163 ● SEP 2017

US Army Research Laboratory

Development of Cranial Bone Surrogate Structures Using Stereolithographic Additive Manufacturing

by Thomas A Plaisted
Weapons and Materials Research Directorate, ARL

by Jared M Gardner
Bennett Aerospace Inc, Cary, NC

REPORT DOCUMENTATION PAGE

Form Approved
OMB No. 0704-0188

1. REPORT DATE *(DD-MM-YYYY)*	2. REPORT TYPE	3. DATES COVERED (From - To)
September 2017	Technical Report	Jan 2015 to Feb 2017

4. TITLE AND SUBTITLE
Development of Cranial Bone Surrogate Structures Using Stereolithographic Additive Manufacturing

5a. CONTRACT NUMBER

5b. GRANT NUMBER

5c. PROGRAM ELEMENT NUMBER

6. AUTHOR(S)
Jared M Gardner and Thomas A Plaisted

5d. PROJECT NUMBER

5e. TASK NUMBER

5f. WORK UNIT NUMBER

7. PERFORMING ORGANIZATION NAME(S) AND ADDRESS(ES)
US Army Research Laboratory
ATTN: RDRL-WMM-A
Aberdeen Proving Ground, MD 21005-5066

8. PERFORMING ORGANIZATION REPORT NUMBER
ARL-TR-8163

9. SPONSORING/MONITORING AGENCY NAME(S) AND ADDRESS(ES)

10. SPONSOR/MONITOR'S ACRONYM(S)

11. SPONSOR/MONITOR'S REPORT NUMBER(S)

12. DISTRIBUTION/AVAILABILITY STATEMENT
Approved for public release; distribution is unlimited.

13. SUPPLEMENTARY NOTES

14. ABSTRACT
We report on the use of stereolithographic (SLA) additive manufacturing to create surrogate structures to mimic the layered construction and porous internal structure of the human cranium. Surrogate structures were designed to replicate the solid volume and thickness of the diploë and inner and outer tables typical of human cranial bones. Pore structures in the diploë region were created based upon a repeating unit cell, whereby the pore diameter and pore wall thickness were tuned to reproduce the target level of porosity, while remaining within dimensions that could be reasonably reproduced using the SLA process. Three candidate pore structures were fabricated using a low modulus, transparent material that was chosen for to aid in the development and evaluation of the primary fabrication and postprocessing conditions. When tested in flexure, the surrogate structures exhibited a range of responses in terms of beam stiffness and failure characteristics that resembled failure modes observed in similar beam testing of cranial bone.

15. SUBJECT TERMS
tissue surrogates, cranial bone, stereolithography, additive manufacturing, pore structure

16. SECURITY CLASSIFICATION OF:			17. LIMITATION OF ABSTRACT	18. NUMBER OF PAGES	19a. NAME OF RESPONSIBLE PERSON
a. REPORT	b. ABSTRACT	c. THIS PAGE			Thomas A Plaisted
Unclassified	Unclassified	Unclassified	UU	26	19b. TELEPHONE NUMBER (Include area code) 410-306-4960

Standard Form 298 (Rev. 8/98)
Prescribed by ANSI Std. Z39.18

Contents

List of Figures

List of Tables

Preface

The research reported in this document was performed in connection with contract/instrument W911QX-16-D-0014-0002 with the US Army Research Laboratory. The views and conclusions contained in this document are those of the authors and should not be interpreted as presenting the official policies or position, either expressed or implied, of the US Army Research Laboratory or the US Government unless so designated by other authorized documents. Citation of manufacturer's or trade names does not constitute an official endorsement or approval of the use thereof. The US Government is authorized to reproduce and distribute reprints for Government purposes notwithstanding any copyright notation hereon.

Acknowledgments

We would like to acknowledge Jacob Schimelman for assistance with the tensile testing and Jennifer Sietens for acquiring the microcomputed tomography images reported herein.

1. Introduction

Injury and survivability assessments are critical to the design and success of protective systems for the Soldier. The validity of the assessments depends on the quality of the human surrogates, which may involve the use of anthropomorphic test devices (ATDs) or postmortem human subjects (PMHSs). ATDs are used most frequently because they can be easily instrumented and are high durable. However ATDs lack the biofidelity of human anatomy. The constituent materials often fail to replicate important properties such as density, stiffness, fracture toughness, wave speed, and others that are essential to capturing the response of materials under dynamic loading conditions.[1,2] Without these properties, the ATD is unable to reproduce realistic loading paths through the body both before and after tissue failure. Alternatively, testing with a PMHS improves the level of biofidelity but comes with inherent uncertainties caused by variability in donor tissue. The development of synthetic surrogate tissues that reproduce the underlying biological material response in a repeatable, consistent manner will improve the fidelity while also reducing experimental uncertainty. Toward this goal, we aim to create synthetic materials that mimic the mechanical response of human cranial bone in both constituent material behavior as well as microstructure. Developments in additive manufacturing (AM) and materials provide an opportunity for creating surrogates with detailed, organic features similar to those observed in cranial bone.

1.1 Cranial Bone

Cranial bone is unique in its characteristic 3-layer sandwich construction, consisting of hard cortical bone on the inner and outer surfaces, known as the tables, with a porous region in the middle. The porous region is also referred to as trabecular bone and, specifically in the cranial vault, this region is called the diploë. The material constitution of the bone is same across these layers, consisting of hydroxyapatite, collagen, and water. On a macroscopic scale, the gradient in porosity gives the appearance of 3 layers, though there is no distinct demarcation when inspecting the microstructure. Unlike the load-bearing bones of the legs, the cranial bone does not exhibit any significant anisotropy in mechanical properties. For this reason, cranial bone is a suitable candidate for early surrogate material and processing development.

A thorough characterization of cranial bone microstructure has been completed at the US Army Research Laboratory.[3] The study focused on the parietal and frontal bones extracted from 4 adult male PMHSs aged between 76 and 86. Microcomputed tomography (CT) was used to characterize the porosity through the

thickness of each bone to generate porosity-depth profiles, as shown in Fig. 1. The thickness of the tables and diploë layers were also measured, where a porosity greater than 30% was chosen as the metric to define the transition. Table 1 summarizes the overall thickness of the parietal and frontal bones and the proportion of the thickness comprising the tables and diploë. While these values serve as guidelines when defining dimensions for the development of surrogate cranial bone designs, it should be noted that human cranial bone exhibits significant variability in architecture and mechanical response among similar populations.[4]

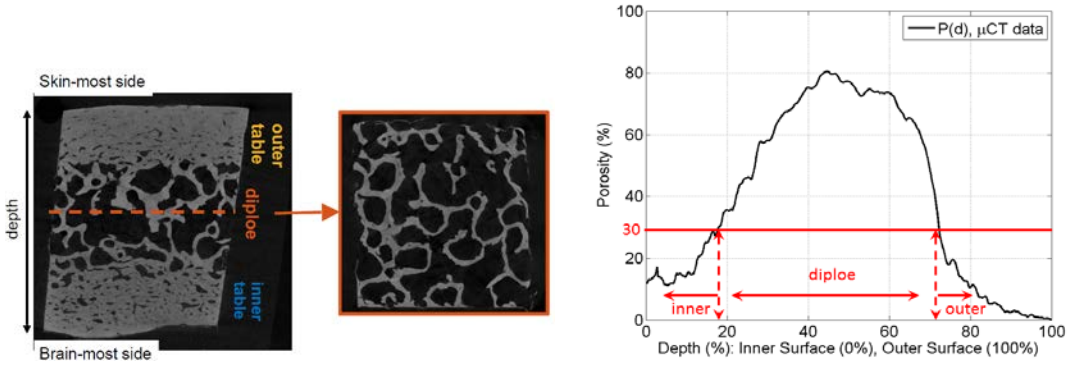

Fig. 1 (Left) CT images of a sample of cranial bone illustrating the characteristic 3-layer sandwich structure and associated porosity. (Right) Porosity as a function of depth from inner to outer surface of the skull.[3]

Table 1 Summary of dimensions measured for parietal and frontal bones tabulated from Alexander et al.[3]

Thickness	Parietal bone	Frontal bone
Overall (mm)	6.7 ± 1.3	8.4 ± 1.4
Outer table (%)	19.4 ± 6.3	22.7 ± 2.7
Diploë (%)	66.0 ± 9.8	43.2 ± 11.9
Inner table (%)	14.6 ± 4.7	34.1 ± 12.0

Advances in medical imaging allow us to generate detailed 3-D digital models of human bone structures. These models in theory can then form the basis of computer-aided design (CAD) files that are used to print anatomical surrogates. However, limitations in printing resolution precludes the reproduction of micronscale features while the random, organic nature of these structures poses further challenges to the manufacturing process. While this approach may eventually prove to be the most biofidelic, we also consider the development of a generic architecture that captures the salient features of the sandwich structure in human cranial bone.

1.2 Additive Manufacturing (AM)

AM, in particular stereolithography (SLA), may be a potential direct manufacturing pathway to development of synthetic surrogate human tissues. Reproducing the micronscale features that typify trabecular bone requires high-resolution manufacturing methods, which makes SLA one of the best suited compared to other AM techniques at present. In our previous work, we have used SLA to evaluate materials that may be suitable mechanical surrogates for cranial cortical bone.[5,6] In this work, we focus on the design and processing of a surrogate pore structure to mimic the diploë. Therefore, the material used in this study was chosen for its ease of processing, availability, and moderately high mechanical properties. In the future, we plan apply the design and manufacturing approaches developed in this study to manufacturing surrogates using a more biofidelic material. The primary objective of this study is to develop a methodology for the design and manufacturing of structures with biomimetic responses, like those of human cranial tissue.

2. Method

2.1 Materials

Somos WaterShed XC 11122 (DSM Functional Materials, Elgin, IL) was used to create bone-like sandwich structures via AM. XC 11122 is a commercially available, unfilled, acrylonitrile butadiene styrene (ABS)-like photopolymer material system, specifically designed for SLA processing. XC11122 has a high degree of optical clarity in the cured state, which allowed qualitative assessments of the part build to be made visually during processing. This material has acceptable structural rigidity for the purpose of developing the AM processing techniques in this study. However, the strength and stiffness of this material are well below that of human bone and thus do not make it a suitable candidate as a surrogate material. Mechanical properties for XC-11122 are provided in Table 2 along with typical property values cited for the cortical bone in the human cranium.

Table 2 Material properties of Somos XC 11122

Somos XC 11122	Density (g/cm^3)	Tensile modulus (GPa)	Flexural modulus (GPa)	Tensile strength (MPa)	Flexural strength (MPa)
Manufacturer[a]	1.12	2.77	2.21	50.4	68.7
As-tested	1.16[b]	2.69[c]	2.36[d]	56.5[c]	73.7[d]
Human cranial cortical bone	1.8[e]	12.6[f]	6.2[g]	72[f]	85[h]

Notes: [a]DSM S[7]
[b]ASTM[8]
[c]ASTM[9]
[d]ASTM[10]
[e]Peterson and Dechow[11]
[f]Wood[12]
[g]Auperrin et al.[13]
[h]Motherway et al.[4]

2.2 Sample Design

In this report, we focus on porosity as a key characteristic to reproduce in the bone surrogate structures, since the strength and stiffness of human bone is inversely proportional to its porosity.[4,14] Reproducing the thickness of the 3-layer structure likewise has a great effect on mechanical response and serves as a key design parameter. The layer thicknesses and ranges in porosity we seek to reproduce in the surrogate structures are given in Table 3. These characteristics were chosen based upon a survey of cranial bone properties cited in the literature,[3,4,11–13] while also keeping the initial design parameters within the limitations of current AM processing capabilities.

Table 3 Thickness dimensions of the tables and diploë and associated porosity ranges targeted for the first-generation designs

	Thickness (mm)	Porosity
Outer table	1.7	0
Diploë	2.8	~40%–80%
Inner table	1.7	0
Total	6.2	~20%–35%

The design of our first surrogate bone structure uses a unit cell approach for generating sandwich-like porous structures. The unit cell is used to create highly simplified geometries that are used for initial manufacturing and modeling studies of these types of structures. For simplicity, the initial designs do not include curvature or variation in thickness within each layer.

The unit cell has 6 variable parameters in rectangular Cartesian (x-y-z) coordinates including 3 sides and 3 radii. In the first generation of these structures, the variables are reduced from 6 to 2, in that the structures are cubic and have pores of uniform

radii. Figure 2 shows the CAD model of the simple rectangular unit cell that was used to generate the open cell porosity representing the diploë region. This unit cell was repeated in the x, y, and z directions by using a patterning feature in the CAD software. Finally, the solid outer surface tables were added to the model. The overall dimensions of the structure in the width, length, and thickness are customizable, as are the dimensions of the pore wall thickness, *a*, and radius, *r*, the number of pore layers, and thickness of solid outer surfaces.

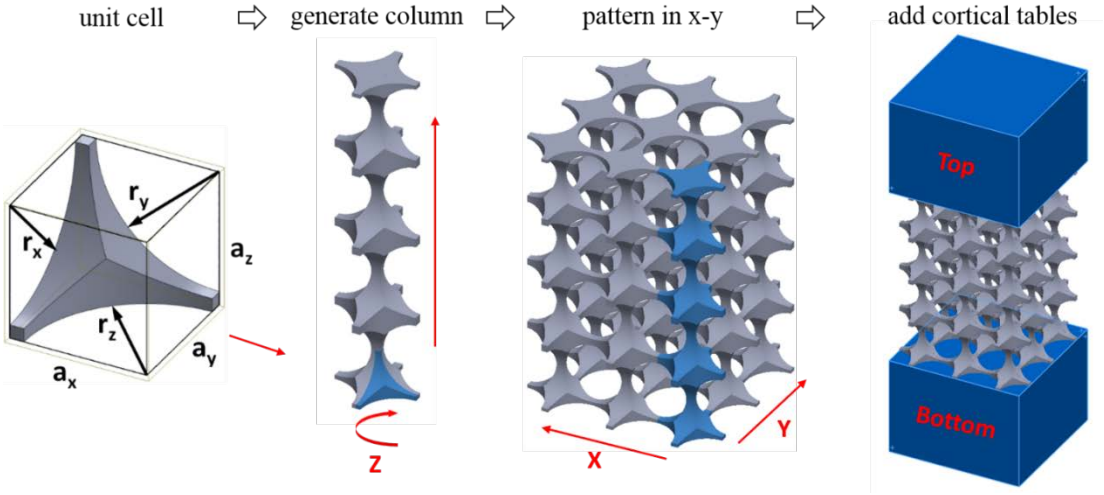

Fig. 2 CAD process for generating the bone-like sandwich structures

Using this design process, Fig. 3 illustrates how pore diameter, pore wall thickness, and number of pore layers through the thickness relate to total solid volume in the porous region. Considering our target values and manufacturing limitations we have focused on 3 designs, designated here as A, B, and C, with characteristics listed in Table 4 and illustrated in Fig. 4.

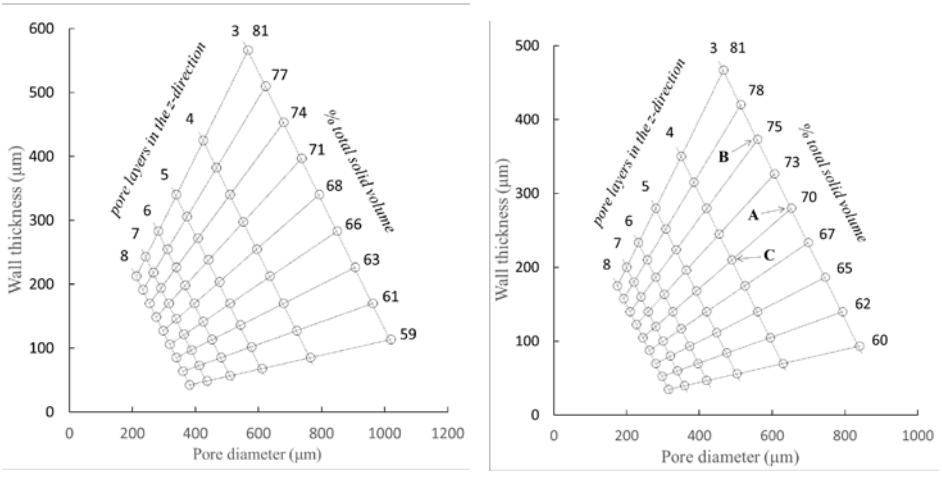

Fig. 3 Design space for the ordered structures, (left) generalized by wall thickness and pore diameter, and (right) the first-generation design space (sample designs A, B, and C are labeled)

Table 4 Characteristics of the pore structure for surrogate structures fabricated

Design	Total solid volume (%)	Total porosity (%)	No. of pore layers	Pore diameter (μm)	Pore wall thickness (μm)
A	70	30	3	653	280
B	75	25	3	560	373
C	75	25	4	490	210

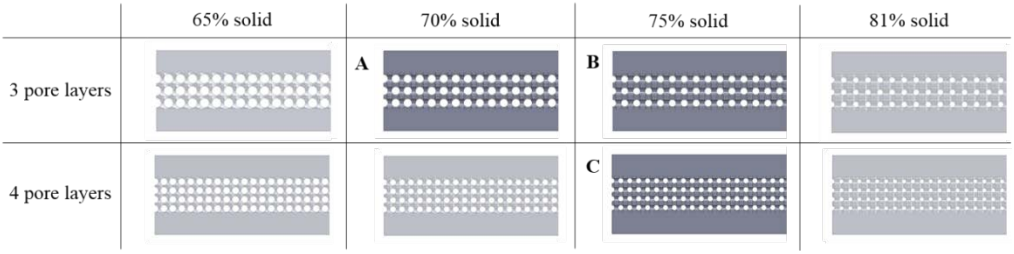

Fig. 4 Select cross-sectional views of design 1 variants with 3 and 4 layers of pores. Sample designs A, B, and C are shown in darker color.

The first-generation structures are low complexity, highly ordered geometries, and have the following basic characteristics:

1) Flat surfaces/no curvature
2) Constant cross-sectional thickness
3) Solid cortical region (disregarding typical void content due to SLA processing)
4) Highly ordered trabecular region based on single repeating unit cell of constant radii

Future designs could systematically incorporate higher levels of complexity such as nonspherical pores and porosity gradients. Computational modeling and simulation can be combined with statistical analysis of tested mechanical properties in order to identify the most influential design parameters affecting structural response.

2.3 Processing

The sandwich structures were produced via SLA AM using a Viper-Si (3D Systems, Rock Hill, SC). A typical SLA machine cyclically raises and lowers a platform on which the parts are fabricated in a bath of photosensitive liquid resin, as shown in Fig. 5. With each cycle, a blade is passed across the platform to create a uniform layer of resin. The resin layer is exposed to a UV laser that traces a cross section of the desired geometry, thereby selectively curing the resin into a specific

pattern. The process is repeated as the platform is lowered into the resin and the next layer is cured on top of the previous layer.

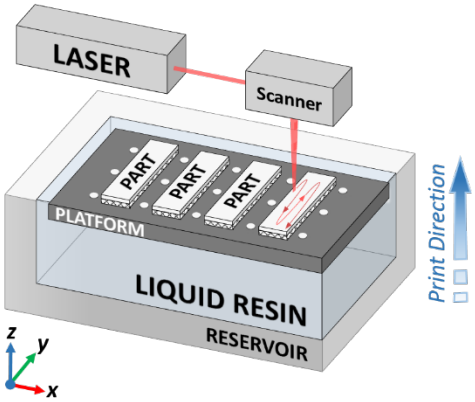

Fig. 5 Schematic of the SLA AM process

In fabricating each structure, files specific to each surrogate pore design were exported from the CAD software as .stl files. These files were then preprocessed within 3D Lightyear (version 1.4) software using building parameters (style files) specific to the XM 11122 polymer system and Viper-Si and subsequently loaded into the Viper-Si for fabrication using software 3D Systems Buildstation (version 5.5.1). Parts were printed using the high-resolution setting of the Viper with an incremental layer thickness of 0.040 inch. The temperature of the resin bath was maintained at 30 °C.

Postprocessing and cleaning of the parts is a significant manufacturing challenge for porous structures. Uncured polymer, trapped within the internal porous volume, must be removed prior to postcure. Typical methods involve solvent washing, but care must be taken to remove the uncured polymer without degrading of the structure. Pores under roughly 1000 μm diameter required multiple solvent washing iterations, during which the optical transparency of the cured XM 11122 polymer was a tremendous asset for determining when the resin had been removed.

The cleaning process consisted of initially applying compressed air to remove excess resin from the porous region of the specimen. Specimen were submerged in a bath of isopropyl alcohol (IPA) and attached via wire mesh to a magnetic stirring bar. The stirring bar was rotated at about 600 rpm for 15 min, after which the specimen were removed and again subjected to compressed air. This was followed by another soak with agitation in IPA for 5 min and final exposure and drying under compressed air. The final step of processing was to postcure the samples in a UV oven. Postcuring was performed in a 3D Systems Model 300 oven for 30 min.

Studies were conducted to evaluate manufacturing feasibility using square-shaped samples. The size of the design 1 variants A, B, and C was scaled uniformly in all directions by 200%, printed, cleaned, and postcured. This process was repeated at scales of 175%, 150%, 125%, and finally 100%, as pictured in Fig. 6.

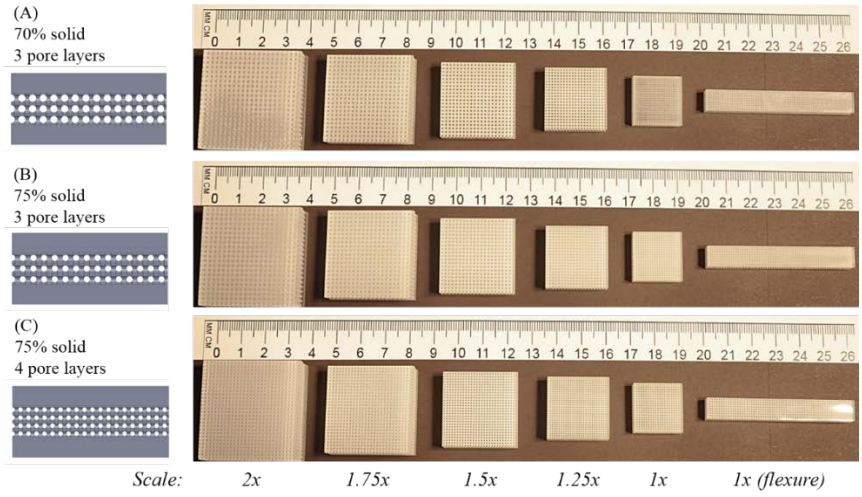

Fig. 6 Physical samples fabricated by SLA with surrogate pore designs A, B, and C

2.4 Micro-CT Analysis

Micro-CT analysis of printed structures was performed on select samples post processing. Images (Fig. 7) were obtained on a Skyscan 1072 micro-CT with the following settings: 40 kV, 3 W (75 mA), 4.2479-µm voxel size, 3-s exp time, and 1601 projections.

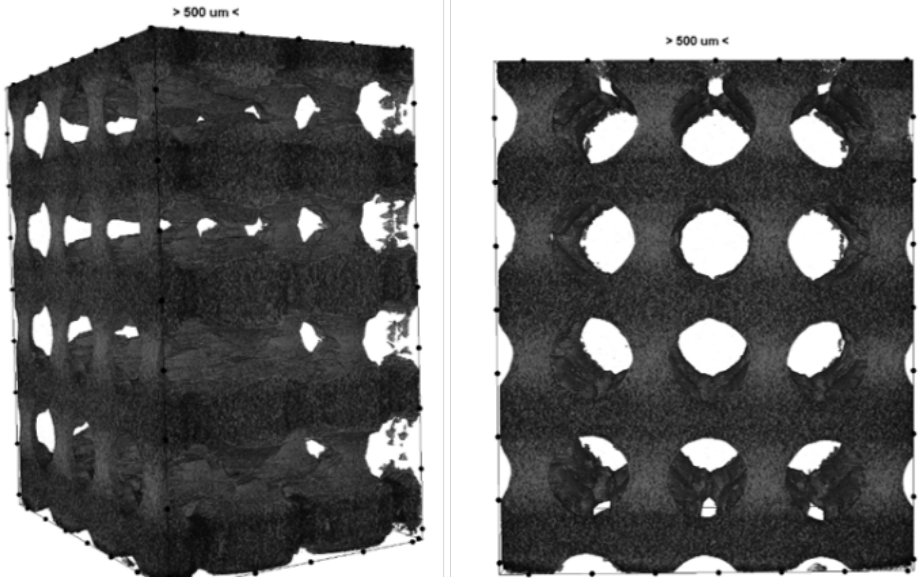

Fig. 7 Micro-CT images of the pore structure for design A

3. Results

3.1 Tensile Testing

Tensile testing of the polymer system Somos 11122 was performed according to ASTM D638-10.[9] Specimens were printed in a dumbbell geometry with a nominal thickness of 3 mm. Instron model 1125B electromechanical frame with a 1 kip load cell was operated in displacement control at a rate of 5 mm/min. Strain was measured by digital image correlation (DIC), using a digital camera (Grasshopper model, Point Grey Inc.). Tensile dumbbell specimen were fabricated in 2 orientations: flat type specimens (quantity 6) were made such that layer-by-layer deposition coincided with the smallest dimension of the dumbbell tensile geometry (thickness), and edge type specimens (quantity 3) in which the deposition occurred across the face of the geometry, as illustrated in Fig. 8. Tensile response curves are shown in Fig. 9.

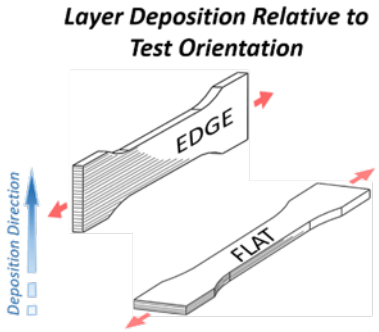

Fig. 8 Orientation of polymer layer deposition relative to dumbbell geometry for edge and flat specimen types

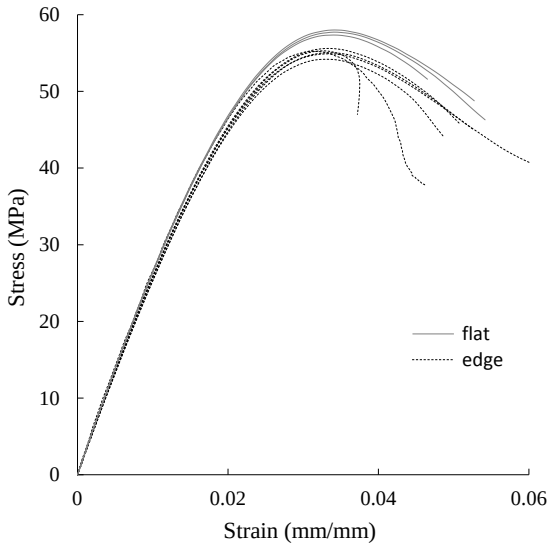

Fig. 9 Tensile test results for Somos WaterShed XC 11122 photopolymer in edge and flat printed orientations

3.2 Flexural Beam Testing

Flexural testing of the surrogate porous designs was performed according to ASTM D790-10.[10] Testing was performed using an Instron model 1125B electromechanical frame with a 1 kip load cell. Samples were displaced at a rate of 0.1 mm/min. The span of the 3-point bending fixture was 50 mm and diameter of the loading pins was 5 mm.

Sandwich beams based on pore designs A, B, and C were fabricated out of material XC 11122 photopolymer with nominal length of 60 mm and width of 8.3 mm. The total thickness of each beam was 6.2 mm, where the outer faces consisted of solid faces 1.7 mm thick and the central porous region was 2.8 mm thick, such that the span-to-depth ratio was 8. Additional beams without central porous regions were fabricated for comparison. These beams had nominal dimensions 60 mm length, 12.7 mm width, and 3 mm thickness, such that the span-to-depth ratio was 16.3.

Figure 10 shows the flexural response of surrogate designs A, B, and C versus that of the solid beam. Photographs typical of the failure patterns of the beams are given in Fig. 11.

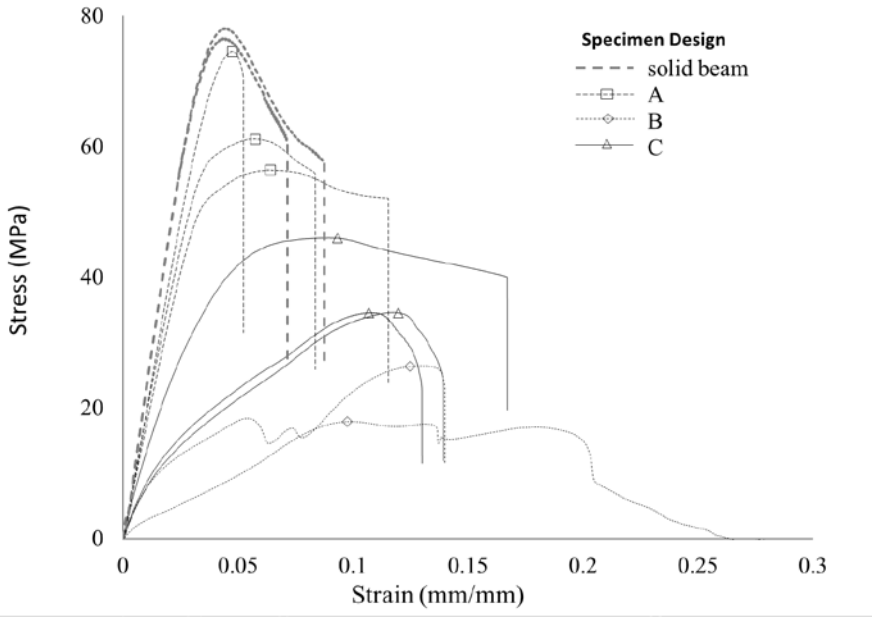

Fig. 10 Flexural response of surrogate designs A, B, and C compared to that of a solid beam of the same material

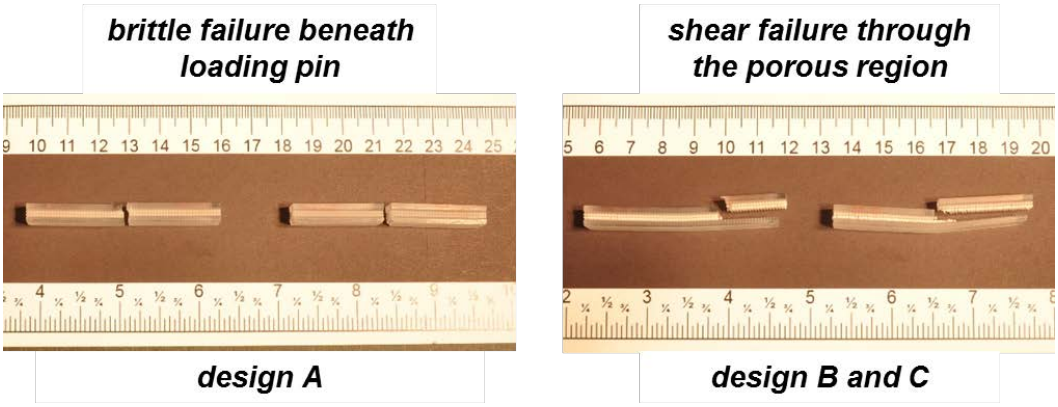

Fig. 11 Photographs of flexural beams post failure. Design A failed directly beneath the loading pin (left). Design B and C failed is a shear mode through the porous region of the beam (right).

4. Discussion

Three candidate porous architectures were designed and fabricated to mimic the physical characteristics of human cranial bone. Micro-CT imaging of one of those architectures (design A) indicate that the SLA manufacturing successfully produced porous structures as intended. Furthermore, the postprocessing conditions were able to remove the majority of residual resin in the internal structure.

The tensile modulus of the edge printed specimens was 2.64 ± 0.03 GPa, slightly lower than that of the flat printed orientation, which had a modulus of 2.72 ± 0.3 GPa. However, the tensile strength of the edge specimens (55.0 ± 0.48 MPa) was higher than that of the flat specimens (57.7 ± 0.03 MPa). This result indicates some processing induced anisotropy is introduced due to the direction in which the layers are deposited. In both cases, the sequential layers run parallel to the loading direction of the tensile specimen. Prior studies in a particle reinforced material processed by the same machine have also observed a modest variation due to the processing direction, which was attributed to unequal distribution of reinforcement in the material.[5] The 11122 material does not contain any particle reinforcement, however. The source of this difference requires further investigation. Despite this variation, the general the tensile response was similar to that as quoted by the manufacturer, as listed in Table 2. The average tensile modulus was slightly lower than that of the manufacturer while the tensile strength was slightly higher but values were in the expected range.

Flexure response of the solid polymer beams was also similar though slightly higher in terms of both flexural modulus and strength compared to that stated by the manufacturer. Postcuring conditions can have an effect on modulus and strength, which may explain the difference, though postcure conditions were not specified on the manufacturer datasheet.

The flexural response of the beams that incorporated the surrogate pore structures revealed a range of responses resulting from the design of the pore structure. Since the surrogate structures were identical in all respects except middle section, we conclude that the design of the porous region dictated the bending response. As expected, the solid sample without porosity exhibited a linear fracture response, with some yielding behavior but mostly brittle failure. Fracture propagated directly through the thickness of the specimen at a location below the central loading pin. A similar response was observed for surrogate design A. The other architectures, B and C, were not as stiff and exhibited a more gradual failure response, with some specimen straining to as much as 20%–25% before eventual failure. In these cases, the failure initiated on one face of the flexure specimen, propagated laterally through the porous region, before eventually severing the sample into 2 pieces without penetrating into the other face of the flexure specimen.

Interestingly, a similar behavior has been observed in the 3-point bending of cranial specimen. Delille et al. performed flexural testing on 380 beam specimens extracted from the parietal, frontal, temporal, and occipital regions of 20 human craniums.[17] Representative force-displacement traces are shown in Fig. 12. In 93% of the cases, the beam specimen exhibited brittle failure and fractured directly beneath the loading pin. In the remaining 7% of the specimens, the flexural modulus was

significantly lower and the failure much more gradual as the crack initiated from the inner table, propagated laterally through the diploë region before eventually fracturing into 2 pieces.

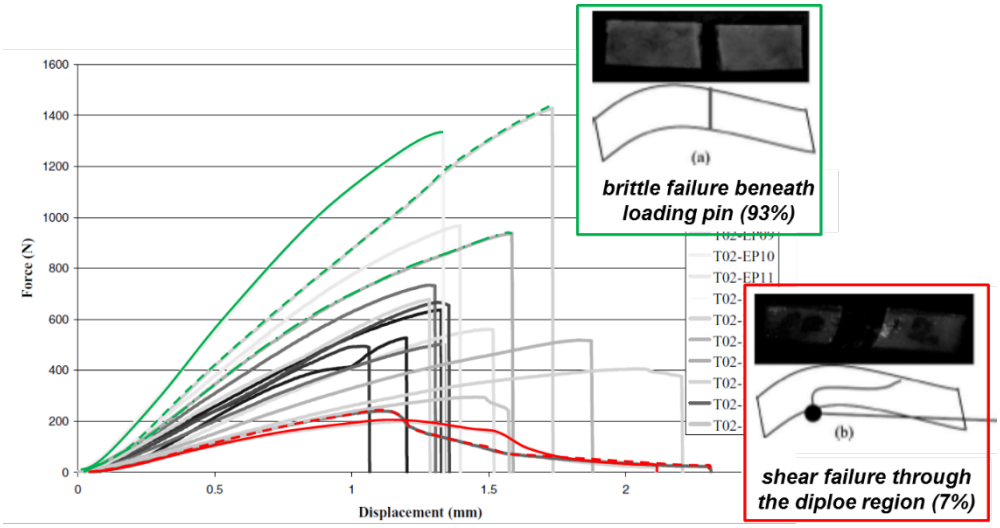

Fig. 12 Force-displacement traces for 3-point bend flexure of cranial bones. The 2 dominant failure modes observed are highlighted.[17]

We note the similarity in the range of flexural responses observed in the surrogate structures. The response of the solid beam and that of design A (70% solid volume, 650-µm pore diameter, 3 pore layers through-thickness) behaved like the majority of the tests performed by Delille et al. The beam possessed sufficient flexural rigidity, resulting from the shear strength of the pore design, to support significant load, and upon tensile failure of the lower face, strain energy was rapidly released and caused a crack to propagate directly through the beam.

In contrast, design B (75% solid volume, 560-µm pore diameter, 3 pore layers through-thickness) and C (75% solid volume, 420-µm pore diameter, 4 pore layers through-thickness) failed in the same progressive manner as the more compliant beams tested by Delille et al. The shear strength of the pore region led to a low flexural rigidity causing the beam to deflect significantly under relatively low loads, and upon fracture of the lower face the crack progressively separated the core from the face until eventual failure.

The features of each structure that controlled the response are still under investigation. The higher solid content of designs B and C should make them stronger rather than weaker compared to design A. However, designs B and C consisted of the smallest pore diameters. These features may have too small to reproduce accurately with SLA, thus resulting in a weakened structure particularly

at the interface between the face and the core. These theories are the subject of further investigation as we fabricate additional designs as shown in Fig. 3.

5. Conclusions

We have demonstrated the use of SLA AM to create surrogate structures to mimic the layered construction and porous internal structure of the human cranium. Surrogate structures were designed to replicate the solid volume and thickness of the diploë and inner and outer tables typical of human cranial bones. Pore structures in the diploë region were created based upon a repeating unit cell, whereby the pore diameter and pore wall thickness were tuned to reproduce the target level of porosity, while remaining within dimensions that could be reasonably reproduced using the SLA process. Structures with solid volume content of 70% and 75% were designed and fabricated using the SLA process. A low modulus, transparent material was chosen for initial fabrication of the structures to aid in the development and evaluation of the primary fabrication and postprocessing conditions to ensure removal of residual liquid resin. When tested in flexure, the surrogate structures exhibited a range of responses in terms of beam stiffness and failure characteristics. While the material was not intended to mimic the much higher stiffness of human bone, the qualitative failure response did resemble the 2 failure modes observed in similar beam testing of cranial bone. As such, these results support further design, fabrication, and testing of surrogate architectures made with this material as well as materials that more closely match the mechanical properties of cranial bone. Future designs could systematically incorporate higher levels of complexity such as porosity gradients and simulated gradients. Computational modeling and simulation can be combined with statistical analysis of tested mechanical properties to identify the most influential design parameters affecting structural response.

6. References

1. Crandall JR et al. Human surrogates for injury biomechanics research. Clinical Anatomy. 2011;24(3):362–371.

2. Payne T, Mitchell S, Bibb R. Design of human surrogates for the study of biomechanical injury: a review. Critical Reviews in Biomedical Engineering. 2013;41(1):51–89.

3. Alexander SL, Rafaels K, Gunnarsson CA, Weerasooriya T. Morphological characterization of the frontal and parietal bones of the human skull. Aberdeen Proving Ground (MD): Army Research Laboratory (US); 2017. Report No.: ARL-TR-7962. p. 78.

4. Motherway JA, Verschueren P, Van der Perre G, Vander Sloten J, Gilchrist MD. The mechanical properties of cranial bone: The effect of loading rate and cranial sampling position. J Biomechanics. 2009;42(13): 2129–2135.

5. Plaisted TA, Gardner JM, Gair JL. Characterization of a composite material to mimic human cranial bone, Aberdeen Proving Ground (MD): Army Research Laboratory (US); 2015. Report No.: ARL-RP-0552.

6. Plaisted T, Gunnarsson A, Sanborn B, Weerasooriya T. Dynamic fracture response of a synthetic cortical bone simulant. In: SEM XII International Congress. Orlando (FL): Society for Experimental Mechanics; 2016.

7. DSM S. Somos WaterShed XC 11122 technical data. 2017 [cited 2017 Aug 16].

8. ASTM_International. Standard test methods for density and specific gravity (relative density) of plastics by displacement, in D792–08. West Conshohocken (PA): ASTM International; 2008. p. 6.

9. ASTM_International. Standard test method for tensile properties of plastics, in D638–10. West Conshohocken (PA): ASTM International; 2010. p. 16.

10. ASTM_International. Standard test methods for flexural properties of unreinforced and reinforced plastics and electrical insulating materials, in ASTM D790-10. West Conshohocken (PA): ASTM International; 2017. p. 12.

11. Peterson J, Dechow PC. Material properties of the inner and outer cortical tables of the human parietal bone. The Anatomical Record. 2002;268(1):7–15.

12. Wood JL. Dynamic response of human cranial bone. J Biomechanics. 1971;4(1):1–12.

13. Auperrin A, Delille R, Lesueur D, Bruyère L, Masson C, Drazétic P. Geometrical and material parameters to assess the macroscopic mechanical behaviour of fresh cranial bone samples. J Biomechanics. 2014;47(5):1180–1185.

14. Carter D, Hayes W. The compressive behavior of bone as a two-phase porous structure. JBJS. 1977;59(7):954–962.

15. Hubbard RP. Flexure of layered cranial bone. J Biomechanics. 1971;4(4):251–263.

16. Wood JL. Mechanical properties of human cranial bone in tension. Ann Arbor (MI): University of Michigan; 1969. p. 108.

17. Delille R, Lesueur D, Potier P, Drazétic P, Markiewicz E. Experimental study of the bone behaviour of the human skull bone for the development of a physical head model. Intl J Crashworthiness. 2007;12(2):101–108.

18. Peterson J, Dechow PC. Material properties of the human cranial vault and zygoma. Anat Rec A Discov Mol Cell Evol Biol. 2003;274(1):785–97.

19. McElhaney JH, Fogle JL, Melvin JW, Haynes RR, Roberts VL, Alem NM. Mechanical properties of cranial bone. J Biomechanics. 1970;3(5):497–511.

List of Symbols, Abbreviations, and Acronyms

3-D	3-dimensional
ATD	anthropomorphic test device
CAD	computer-aided design
CT	computed tomography
IPA	isopropyl alcohol
PMHS	postmortem human subject
SLA	stereolithography
UV	ultraviolet

1 (PDF) DEFENSE TECHNICAL INFORMATION CTR DTIC OCA

2 (PDF) DIR ARL RDRL CIO L IMAL HRA MAIL & RECORDS MGMT

1 (PDF) GOVT PRINTG OFC A MALHOTRA

1 (PDF) ARL RDRL WMM A T PLAISTED